

Article

Studies of Carbon Incorporation on the Diamond {100} Surface during Chemical Vapor Deposition using Density Functional Theory

Andrew Cheesman, Jeremy N. Harvey, and Michael N. R. Ashfold

J. Phys. Chem. A, **2008**, 112 (45), 11436-11448 • DOI: 10.1021/jp8034538 • Publication Date (Web): 07 October 2008

Downloaded from <http://pubs.acs.org> on February 19, 2009

More About This Article

Additional resources and features associated with this article are available within the HTML version:

- Supporting Information
- Access to high resolution figures
- Links to articles and content related to this article
- Copyright permission to reproduce figures and/or text from this article

[View the Full Text HTML](#)



ACS Publications
High quality. High impact.

Studies of Carbon Incorporation on the Diamond {100} Surface during Chemical Vapor Deposition using Density Functional Theory

Andrew Cheesman, Jeremy N. Harvey,* and Michael N. R. Ashfold*

School of Chemistry, University of Bristol, Cantock's Close, Bristol, BS8 ITS, U.K.

Received: April 21, 2008; Revised Manuscript Received: June 10, 2008

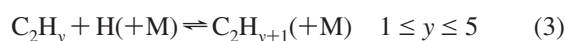
Accurate potential energy surface calculations are presented for many of the key steps involved in diamond chemical vapor deposition on the {100} surface (in its 2×1 reconstructed and hydrogenated form). The growing diamond surface was described by using a large (~ 1500 atoms) cluster model, with the key atoms involved in chemical steps being described by using a quantum mechanical (QM, density functional theory, DFT) method and the bulk of the atoms being described by molecular mechanics (MM). The resulting hybrid QM/MM calculations are more systematic and/or at a higher level of theory than previous work on this growth process. The dominant process for carbon addition, in the form of methyl radicals, is predicted to be addition to a surface radical site, opening of the adjacent C–C dimer bond, insertion, and ultimate ring closure. Other steps such as insertion across the trough between rows of dimer bonds or addition to a neighboring dimer leading to formation of a reconstruction on the next layer may also contribute. Etching of carbon can also occur; the most likely mechanism involves loss of a two-carbon moiety in the form of ethene. The present higher-level calculations confirm that migration of inserted carbon along both dimer rows and chains should be relatively facile, with barriers of ~ 150 kJ mol $^{-1}$ when starting from suitable diradical species, and that this step should play an important role in establishing growth of smooth surfaces.

I. Introduction

Diamond is now grown routinely by chemical vapor deposition (CVD) methods from activated dilute hydrocarbon–hydrogen gas mixtures (typically $< 10\%$ CH $_4$ in H $_2$, $T_{\text{gas}} \approx 3000$ K) on a range of substrates that, typically, are maintained at temperatures in the range $1000 \leq T_{\text{sub}} \leq 1400$ K).^{1–3} The activated gas mixtures contain high densities of atomic hydrogen ($> 10^{16}$ cm $^{-3}$ in the most activated region in a typical 1–2 kW microwave reactor, $> 10^{15}$ cm $^{-3}$ in the immediate proximity of the growing diamond surface, and an order of magnitude or more greater in the case of > 5 kW reactors), which serve to establish dynamic local equilibrium among the various C $_1$ H $_x$ and C $_2$ H $_y$ gas-phase species via a sequence of H-shifting (abstraction and/or addition) reactions^{4–6} of the form:



and



{100} diamond exhibits a cubic morphology, with smooth, flat crystallite surfaces, and low defect densities, ensuring that {100} growth has long been a focus of experimental and theoretical study. The {100} surface in CVD grown material is usually present in a 2×1 reconstructed form, where two surface carbon atoms have relaxed from the bulk positions and moved together to form a C–C bond in the plane of the growing surface.^{7–9} The fully 2×1 reconstructed diamond surface is covered with multiple dimers that are aligned in rows—in contrast to other group XIV semiconductors for which 2×1 reconstruction results in a herringbone pattern of surface dimers.

Many computational studies centered on the {100} surface explored carbon incorporation either by insertion into a reconstructed dimer bond by the ring opening/closing mechanism^{10–16} or via the trough bridging mechanism.¹⁷ Several theoretical papers investigating growth on the {100} surface also explore the effect of heteroatoms.^{11,18,19} Frenklach and co-workers^{20–27} have been at the forefront of exploring the relative probabilities of these two mechanisms, their dependence on process conditions, and the possible role of surface diffusion processes and in developing a consistent model for CVD diamond growth. These studies have focused on CH $_3$ radicals^{23,24} and C $_2$ H $_2$ ^{20,21,25} as growth species, because these are generally considered to be, respectively, the most abundant carbon-containing radical species and the most abundant stable hydrocarbon in the immediate proximity of the growing diamond surface under most CVD conditions.^{4–6} The Frenklach-group studies suggested that CH $_3$ addition to a radical site on a pristine diamond surface is a barrier-less process but that addition of a CH $_3$ radical at a radical site adjacent to a previous incorporation involved surmounting an energy barrier (due to steric hindrance). These findings implied a dominant role for the ring opening/closing mechanism for CH $_3$ radical addition to a reconstructed diamond {100} surface. C $_2$ H $_2$ addition to a surface radical site was also calculated to be energetically feasible under typical CVD conditions, resulting in formation of surface bound $> \text{C}=\text{CH}_2$ species. Skokov et al.²⁵ have discussed how this species might initiate formation of a new diamond layer and could lead to creation of a reconstructed C–C dimer bond at the surface and suggested mechanisms by which this pendant species could be etched back into the gas phase—issues that have been addressed further by Battaile et al.¹² Such arguments have been extended²⁶ to include a degree of mobility for adspecies on the diamond {100} surface; migration of carbon species could help explain the observed propensity for forming smooth diamond {100} surfaces while H atom migration, if permissible, could reduce

* Authors for correspondence. Tel: +44 117 9288312 (M.N.R.A.). E-mail: mike.ashfold@bris.ac.uk. Tel: +44 117 9546991 (J.N.H.). E-mail: Jeremy.Harvey@bristol.ac.uk. Fax: +44 117 9250612.

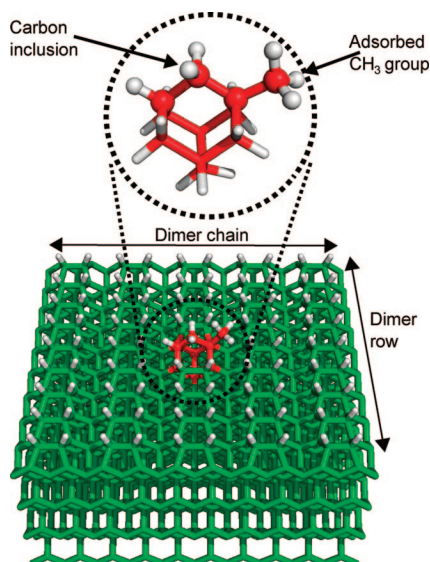


Figure 1. Illustration of the base model used in this study, consisting of a $5 \times 9 \times 4$ slab (defined in terms of numbers of C–C dimer bonds) with a 2×1 reconstructed, H terminated (100) surface. The inset shows an expanded view of the core cluster as red atoms, which are treated in the QM region at the DFT level of theory in many of the calculations, with the unterminated bonds representing link atoms. The extended lattice that is modeled by using MM is shown in green. The QM region in the illustrated case comprises the core C_9 cluster with a CH_2 group incorporated into its C–C dimer bond and a pendant CH_3 group. Key topological features mentioned in the text are labeled.

the effective lifetime of surface radical species, thereby reducing the feasibility of the trough bridging mechanism, for example.

Modeling CVD diamond growth necessarily involves consideration of a large number of elementary gas phase, gas–surface, and surface reactions.²⁸ Initial kinetic investigations focused on the direct incorporation of incident carbon species by using simple adsorption models,^{22,29} which succeeded in reproducing published growth rates but offered little insight into the detailed surface chemistry. The shortcomings of these pioneering studies encouraged progressive expansions of diamond {100} growth modeling, incorporating more complex reaction dynamics including possible etching of surface atoms¹² and surface migrations²⁷ within kinetic Monte Carlo (KMC) protocols.

KMC studies constitute such a major advance in the mesoscopic modeling of diamond growth that it is now opportune to revisit the energetics of various key reactions at higher levels of theory and the boundary conditions that are used as input to such calculations. Here, we present results of density functional theory (DFT) calculations performed in conjunction with a large quantum mechanical/molecular mechanics (QM/MM) cluster model that further explore selected carbon incorporation pathways on the {100} face of diamond.

II. Computational Details

The base QM/MM model of the 2×1 reconstructed, H-terminated, diamond {100} surface used in this work is illustrated in Figure 1. The model consists of a $5 \times 9 \times 4$ slab (defined in terms of numbers of C–C dimer bonds), with an initial geometry that is defined by the bulk diamond lattice points. The positions of the peripheral atoms (with nonchemical stoichiometry) were held frozen during the calculations. The size of the model was chosen after carrying out tests to ensure that it was large enough to minimize stresses in the region described by higher (QM) levels of theory induced by clamping

the perimeter atoms. Also, checks were made to ensure that differences in calculated energies upon changing the model size were smaller than the estimated inaccuracy of the QM method. The initial geometry of the reconstructed surface layer was derived by using the optimized geometry of the C_9H_{14} cluster obtained by using DFT theory (B3LYP) with the 6-311G** basis set,³⁰ arranging the chains of surface dimers as shown in Figure 1 and then allowing the structure to relax to the minimum energy geometry. Subsequent modeling involves a number of different small QM regions connected through link atoms³¹ to the remainder of the structure that is described by molecular mechanics (MM2). The MM2 molecular mechanics protocol employed is optimized for hydrocarbon species and has been parametrized by using diamond within the subsets.³² The size and nature of the QM region used in each QM/MM calculation has been chosen so as to describe all key electronic effects at the QM level. This means that different QM regions are used in different sections of the paper. The precise model used in each case is shown in the figures.

The bulk of the calculations were carried out by using a hybrid QM/MM method by using the QoMMA program, developed in-house.^{33,34} The QM parts of the calculations were performed by using Jaguar,³⁵ and the TINKER program³⁶ was used to model the MM interactions. Given that the present studies focus on radical reactions at the diamond surface, no electrostatic interactions were included between the QM and MM regions. The geometry optimizations were performed by using the B3LYP density functional with the 6-31G* basis set to describe the QM region, and single-point calculations of the QM region at that geometry were then carried out by using the larger (6-311G**) basis set and the resultant energies incorporated into the reported QM/MM results. Some additional single-point energies were calculated at the MP2/6-311G** level of theory. In order to obtain more accurate results, the MP2 correlation energies were spin-component scaled,³⁷ leading to SCS-MP2 energies. In most cases, geometry optimizations were performed by using restricted B3LYP methods for closed- and open-shell species, but unrestricted B3LYP was used for some open-shell diradicals. Hence, total energies from both restricted and unrestricted calculations are used to derive potential energy surfaces (PESs). We have checked for a number of spin-doublet radicals and spin-triplet diradicals that the energy difference between restricted and unrestricted B3LYP calculations is small (<10 kJ mol⁻¹). Approximate transition states (TSs) were determined by mapping the energy along a reaction coordinate, such as a bond length or a difference between two bond lengths. For each successive value of the coordinate, full geometry optimization was carried out by using a harmonic constraint to maintain the system close to the target value of the coordinate. The energy of the highest-lying point along the curve generated in this way corresponds to the energy of the TS. Although this reaction-coordinate driving approach is known to perform poorly in some cases and alternative methods may be preferred,³⁸ good behavior was obtained here, and with the small step size we use, the error involved in locating approximate TSs rather than exact saddle points was estimated to be <1 kJ mol⁻¹. All calculated energies are quoted in kJ mol⁻¹ and have not been corrected for zero-point effects unless stated otherwise.

Additional calculations were performed for the smallest QM region. In this case, QM/MM geometry optimization was carried out by using the B3LYP/6-31G* level of theory followed by single-point calculations by using B3LYP/6-311G** for the QM region. Single-point QM/MM energies were obtained by using the MP2/6-311G** and CCSD(T)/cc-pVTZ levels of theory for

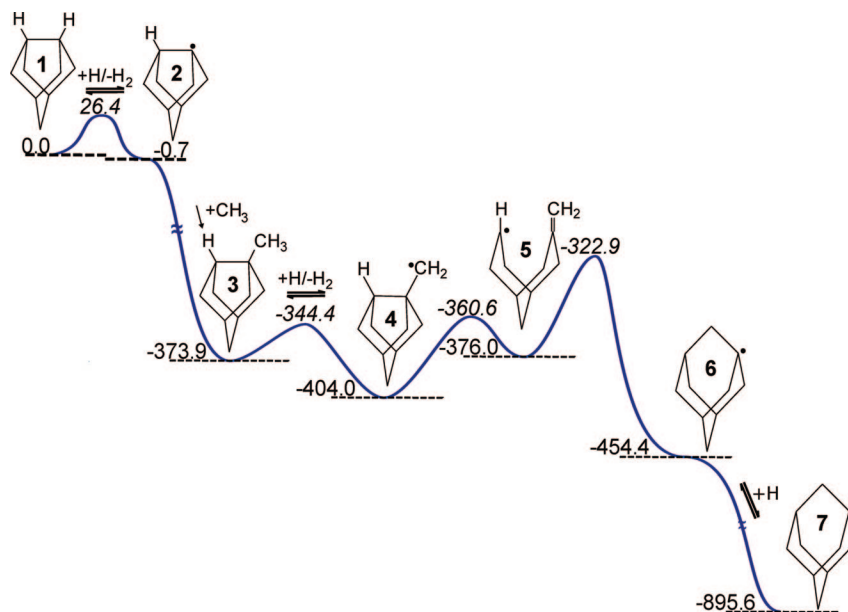


Figure 2. Reaction path for incorporating a CH₂ group into a C–C dimer bond. Energies (B3LYP QM/MM, 6-311G** basis set) are quoted in units of kJ mol⁻¹, relative to that of structure 1. Only the atoms treated in the QM region are shown.

the QM region. In this case, MP2 as well as spin-component scaled³⁷ SCS-MP2 energies are reported below. Pure QM calculations for this small QM region were also carried out. Full geometry optimization was carried out at the B3LYP/6-311G** level of theory, and vibrational frequencies were computed so as to provide zero-point energies. MP2/6-311G**, SCS-MP2/6-311G**, and CCSD(T)/cc-pVTZ single-point energies were computed at the B3LYP geometry. For comparison, the same systems were also optimized at the PM3 level of theory. B3LYP calculations were carried out by using Jaguar 5.0 and Gaussian 03,³⁹ MP2, SCS-MP2, and PM3 calculations were performed by using Gaussian 03, and CCSD(T) calculations were carried out by using MOLPRO 2002.⁴⁰

III. Results and Discussion

This section reports calculated energetics of processes by which carbon (in the form of an incident CH₃ radical) might incorporate into the diamond {100} surface. Guided by the earlier studies of Frenklach and others, three distinct mechanisms are considered: insertion into a reconstructed C–C dimer bond, incorporation (bridging) the trough between successive C–C dimers in a chain, and formation of a new dimer row. Two possible migration mechanisms for CH₂ groups on a diamond {100} surface are also investigated. The conclusions include a qualitative consideration of how these mechanisms combine to account for overall diamond growth. To aid the reader, some of the more widely used terms when describing features of the 2 × 1 reconstructed diamond {100} surface are also illustrated in Figure 1. Reference to a pristine diamond surface in the context of this paper will imply a smooth, 2 × 1 reconstructed, H-terminated diamond {100} surface free of any carbon additions or inclusions.

A. Insertion into a Reconstructed C–C Dimer Bond.

Figure 2 illustrates this classic mechanism for C addition to a diamond {100} surface.^{10,13} Following CH₃ addition to a radical site of the surface dimer unit, the ring opening/closing mechanism is initiated by hydrogen abstraction from this pendant CH₃ (step 3 → 4 in Figure 2). The newly formed CH₂ radical then incorporates into the diamond structure via a ring opening/closing sequence (steps 4 → 5 and 5 → 6) rather than by direct

insertion of the pendant CH₂ into the C–C bond (i.e. stepping directly from structure 4 → 6, for which we (and others¹³) calculate a substantial (~200 kJ mol⁻¹) energy barrier. This mechanism has been revisited in the present QM/MM study, with particular regard to possible effects on the reaction energetics of (i) constraining the QM region within a rigid diamond lattice and (ii) steric interactions from the neighboring surface atoms. Figure 2 shows the relative energies of the various elementary steps involved in the incorporation of a CH₂ group within a C–C dimer bond on a pristine diamond {100} surface, calculated starting from a C₉H₁₄ cluster (identical to that employed in refs 13 and 28) as the base QM unit within the QM/MM protocol. Table 1 compares the values returned by the present QM/MM calculations with equivalent results from DFT calculations (at the same level of theory) by using the bare, unconstrained C₉H₁₄ cluster⁴¹ and with results reported previously. SCS-MP2³⁷ single-point energies are reported also. Test calculations reported below obtained by using a very small QM region suggest that the latter are slightly less accurate than the B3LYP/6-311G** calculations; therefore, our discussion focuses on the B3LYP results. The SCS-MP2 results are nevertheless included, because they provide some independent confirmation of some of the key energetics, for example, the C–C bond formation step 2 → 3 and the rearrangement process leading to carbon incorporation (4 → 6).

The B3LYP QM/MM calculations show the initial H-abstraction process (step 1 → 2) to be virtually thermoneutral ($\Delta E = -0.7$ kJ mol⁻¹, $E_a = 26.4$ kJ mol⁻¹). As Table 1 shows, the derived activation energy accords well with that determined by using the isolated QM cluster and with the value reported by Kang and Musgrave,¹³ but all are significantly smaller than that returned by the MRMP2 calculations of Tamura and Gordon.¹⁶ It is likely that the true energy barrier lies somewhere between the two values, because the B3LYP method slightly underestimates the barrier for related H + hydrocarbon reactions, as shown below.^{13,42} CH₃ addition to the surface radical site is barrierless (step 2 → 3, $\Delta E = -373.2$ kJ mol⁻¹).

Our primary interest is in the activation of this pendant CH₃ (step 3 → 4), but it is worth noting that there are also a number of mechanisms by which this CH₃ group might be released back

TABLE 1: Energy Changes, ΔE , and Activation Energies, E_a , (Both in kJ mol^{-1}) Associated with the Various Elementary Steps Involved in CH_2 Incorporation into the C–C Dimer Bond by the Ring Opening/Closing Mechanism Depicted in Figure 2 Returned by the Present QM/MM Calculations (6-311G Basis Set) and by QM Calculations Starting with the Bare C_9H_{14} Cluster, Compared with Previous Results**

step	present study				MRMP2 (ref 16)	DFT (ref 15)	PM3 (refs 23 and 24)	B3LYP (ref 13)
	QM/MM		cluster					
	B3LYP	SCS-MP2	B3LYP (ref 41)	SCS-MP2				
ΔE_{1-2}	-0.7	25.8	-7.6	24.0	-1.7	-36.7		
TS	26.4	65.7	22.9	68.7	51.0		28.5	
ΔE_{2-3}	-373.2	-405.2	-383.7	-430.2	-372.4	-311.6	-307.9	-351.5
TS								
ΔE_{3-4}	-30.1	-8.5	-20.1	11.5	-34.7	-79.1		-37.6
TS	29.5	69.1	27.6	72.3	45.2		25.1	
ΔE_{4-5}	28.0	82.5	1.4	51.3	74.3		51.8	-2.1
TS	43.4	99.9	49.0	119.1	63.1		64.0	40.2
ΔE_{5-6}	-78.4	-124.3	-52.9	-95.8	-75.7		-100.4	-41.8
TS	53.1	58.7	58.0	77.8	50.6		51.5	59.0
ΔE_{4-6}	-50.4	-41.8	-51.5	-44.5	-1.4	-29.3	-48.6	-43.9
TS	/	/	/	/	/	54.4	/	206.7

TABLE 2: Energetic Comparisons of Small Models of the First Two Steps in the Dimer Insertion Mechanism (i.e. H Abstraction, and CH_3 Addition to the Resulting Radical Site) Calculated by Using PM3 and Three Different QM Methods for (a) the Relevant Gas-Phase Processes ($\text{H} + \text{C}_2\text{H}_6 \rightarrow \text{H}_2 + \text{C}_2\text{H}_5$ and $\text{CH}_3 + \text{C}_2\text{H}_5 \rightarrow \text{CH}_3\text{CH}_2\text{CH}_3$), without ($\Delta E_{\text{gas,e}}$) and with Zero-Point Energy Corrections ($\Delta E_{\text{gas,0}}$), and (b) the Corresponding Steps ($1 \rightarrow 2$ and $2 \rightarrow 3$) When the C–C Unit Is Embedded within a MM Framework in the QM/MM Calculation ($\Delta E_{\text{QM/MM}}$)

reaction	expt.	PM3		B3LYP/6-311G**			MP2/6-311G** SCS-MP2/6-311G**				CCSD(T)-pVTZ				
		ΔE_{gas}	$\Delta E_{\text{QM/MM}}$	$\Delta E_{\text{gas,e}}$	$\Delta E_{\text{gas,0}}$	$\Delta E_{\text{QM/MM}}$	$\Delta E_{\text{gas,e}}$	$\Delta E_{\text{gas,0}}$	$\Delta E_{\text{QM/MM}}$	$\Delta E_{\text{gas,e}}$	$\Delta E_{\text{gas,0}}$	$\Delta E_{\text{QM/MM}}$			
ΔE (H-atom abstraction)	-30 ± 6	-137.3	-82.9	-12.6	-26.6	25.2	19.9	11.3	5.7	-2.9	49.8	41.1	-0.6	-14.8	32.1
TS	30.5 ⁴²			28.1	21.3		74.9	73.8	68.1	67.0			52.2	45.4	
ΔE (CH_3 addition)	-351 ± 7	-276.7	-312.7	-376.2	-338.3	-391.6	-398.8	-391.6	-358.7	-351.5	-410.6	-404.8	-419.8	-379.6	-434.2

into the gas phase. Etching processes are clearly of potential importance given that diamond growth can be reversed under CVD conditions in the absence of a carbon source.¹² Such reactions may also play a role in ensuring smooth surface growth under normal CVD conditions, by removing protrusions on the diamond surface. Direct loss is unlikely given the very large bond energy. One possible carbon loss mechanism involves an $\text{S}_{\text{N}}2$ -type displacement reaction with an H atom incident at the methyl C atom and expulsion as CH_4 . This process is calculated to be exothermic ($\Delta E = -44.8 \text{ kJ mol}^{-1}$) with a substantial barrier ($E_a = 134.4 \text{ kJ mol}^{-1}$). It is also possible to envisage loss of the CH_3 radical itself, via a process that is initiated by abstraction of the neighboring H atom on the same C–C dimer bond. The H-atom loss process is calculated to be essentially thermoneutral, with a modest barrier ($E_a = 23.3 \text{ kJ mol}^{-1}$)—reassuringly similar to that of step $1 \rightarrow 2$ in Figure 1—but the subsequent step involving CH_3 loss and formation of an unsaturated surface dimer bond is highly endothermic ($\Delta E = 278.5 \text{ kJ mol}^{-1}$) and hence unlikely even at high temperature. Previous (more favorable) energetic and rate estimates for this possible loss process were based upon analogy with comparable gas-phase reactions.²⁵ Another possibility involves abstraction of an H atom from a surface-bound methyl group, attachment of a second methyl group, removal of a hydrogen atom, and loss of ethene. This mechanism for removing pendant C_nH_y ($n > 1$) groups²⁸ was studied in our previous work focusing on boron incorporation,³⁰ and the final step, ethene loss, was found to be endothermic by $172.6 \text{ kJ mol}^{-1}$. Being entropically favorable, however, this step was deduced to be favorable in terms of free energy above $\sim 1100 \text{ K}$. All of these processes start from a pendant methyl group species (**3** in Figure 2) and hence assume that the latter exists in equilibrium on the surface.

This is reasonable given that rearrangement to **6** (see below) is exothermic but not very highly so.

Returning to the subsequent processes leading to carbon incorporation, the first step is H abstraction from the pendant methyl group (step $3 \rightarrow 4$). As Table 1 shows, compared with the QM calculations on the bare cluster, the QM/MM calculations return a slightly greater exothermicity but a similar activation barrier for this process.

Given that much of the important previous computational work on growth on the diamond {100} surface has employed the PM3 semiempirical level of theory and that the present DFT results are significantly different in some cases, it was deemed prudent to compare the calculated B3LYP energetics for a small model system with those calculated by using several accurate QM methods (MP2, SCS-MP2,³⁷ and CCSD(T)), as well as by PM3. This has been done both with and without including MM contributions. Table 2 summarizes QM/MM results for the first steps of the dimer insertion mechanism (i.e., H abstraction and CH_3 addition to the resulting radical site) obtained by using a small QM region, comprising just a single reconstructed C–C dimer on the diamond {100} surface. The calculated energies ($\Delta E_{\text{QM/MM}}$) are compared with the results for the corresponding gas-phase mimics (i.e., $\text{H} + \text{C}_2\text{H}_6 \rightarrow \text{H}_2 + \text{C}_2\text{H}_5$ and $\text{CH}_3 + \text{C}_2\text{H}_5 \rightarrow \text{CH}_3\text{CH}_2\text{CH}_3$), calculated by using the optimized B3LYP geometries, ($\Delta E_{\text{gas,e}}$) and with zero-point energy corrections ($\Delta E_{\text{gas,0}}$), and with the experimental (gas-phase) values.^{43,44} PM3 theory is parametrized such that the electronic energies, not including statistical mechanical corrections, reproduce room-temperature enthalpies and therefore contain zero-point energy (and indeed thermal energies) implicitly. As such, they should be similar, but not strictly comparable, to the $\Delta E_{\text{gas,0}}$ values returned by the QM methods. Nonetheless, the present

comparisons suggest that PM3 theory overestimates the stabilities of alkyl radicals. Thus, as Table 2 shows, the PM3 calculations underestimate the C–C bond strength (cf. recommended formation-enthalpy data at 0 K) and overestimate the exothermicity of the gas-phase H-abstraction process. One likely consequence of the former would be that models based on energy landscapes determined by PM3 methods are likely to overestimate the rates of CH₃ loss from a diamond surface. Of the various QM methods, the B3LYP and CCSD(T) calculations (after correction for zero-point energy effects) reproduce the exothermicity of the gas-phase H-atom abstraction reaction from ethane well, whereas MP2 and SCS-MP2 calculations underestimate the reaction exothermicity by ~30 kJ mol⁻¹. As expected,^{13,42} the B3LYP method slightly underestimates the barrier to the hydrogen abstraction, whereas the CCSD(T) method with the medium-sized cc-pVTZ basis set slightly overestimates the barrier. Both MP2 and SCS-MP2 overestimate this barrier significantly (a similar trend is noted for steps 1 → 2 and 3 → 4 in Table 1). All three methods describe the energetics of the C–C bond forming reaction reasonably well. Calibration studies such as those summarized in Table 2 encourage the view that the relative energies returned by the chosen QM/MM protocol are likely to be accurate to ~20 kJ mol⁻¹; furthermore, it is reasonable to anticipate some cancellation of errors when considering multistep reaction pathways.

Returning to Figure 2, the elementary steps discussed thus far involve interaction with the uppermost layer of the QM region only, relatively remote from the surrounding MM region. As expected, our QM/MM and bare cluster calculations show greater energetic differences in the case of the ring opening and closing steps (4 → 5 and 5 → 6, respectively), reflecting the effects of steric interaction with H atoms on the adjacent dimers and steric constraints imposed by the neighboring reconstructions. These limit the relaxation of the ring opened intermediate (5 in Figure 2), restricting the separation between the surface radical and the ethylenic group from 3.00 Å (cluster) to 2.55 Å (QM/MM) and reducing the (internal) angle that the latter group makes with the (100) plane from 105.4° (cluster) to 101.9° (QM/MM). Both of these geometric effects serve to destabilize structure 5 in the QM/MM calculation and encourage formation of the closed ring radical species (6). The presence of an adjacent carbon incorporation (as a bridging CH₂) within the dimer chain is found to have minimal effect upon the incorporation energetics displayed in Figure 2, but an incorporated CH₂ species in an adjacent C–C bond along the dimer row has a major steric consequence, increasing the effective barrier to ring opening/closing and reducing the probability of CH₂ incorporation substantially, reinforcing the earlier findings of Skokov et al.²⁴

Steric interactions slightly weaken the C–H bond formed in 7 upon addition of a hydrogen atom to species 6 (bond-formation energy of -441.2 kJ mol⁻¹ compared to -464.4 kJ mol⁻¹ for the C–H bond-formation process 2 + H → 1). At first sight, this finding might suggest that the carbon atom in 6 is more likely to be present in an activated (radical) form than would be the case for a generic C atom at a reconstructed site. However, under diamond CVD conditions, the fraction of radical sites is not expected to be particularly site dependent. Given the quite broad variation in C–H bond energies for different sites on the growing {100} surface, this is perhaps surprising, but is accounted for by the fact that this fraction is primarily determined by the relative rates of the abstraction (C–H + H → C• + H₂) and addition (C• + H → C–H) reactions, both of which depend only weakly on the C–H bond strength. Note that the rate for the reverse reaction (C• + H₂ → C–H + H) is

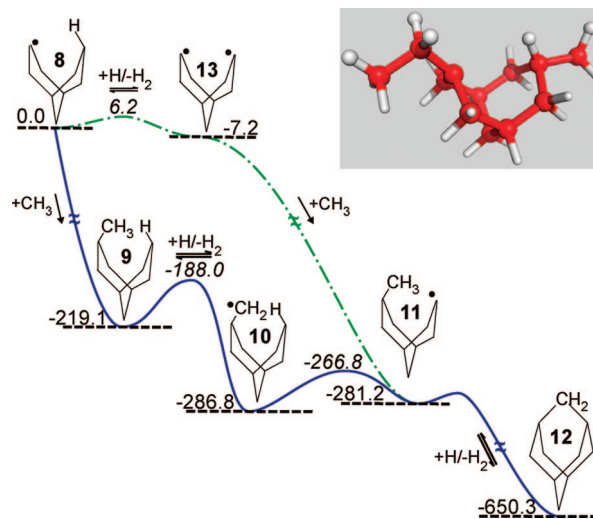


Figure 3. Reaction path(s) for incorporating a CH₂ group across the trough in a dimer chain that has one pre- and postincorporated dimer as immediate neighbors. Energies (B3LYP QM/MM, 6-311G** basis set) are quoted in units of kJ mol⁻¹, relative to that of structure 8. An expanded version of the QM region shown in Figure 4b has been used for these calculations and is shown in the top right-hand corner.

expected to be strongly dependent on the C–H bond strength, but this reaction only makes a minimal contribution to the process of converting surface radical sites into saturated C–H sites, even for the strongest C–H bonds. The fraction of radical sites (compared to terminated surface carbons) is generally considered to be in the range 0.05–0.1 under typical CVD conditions.²⁸

Inspection of Table 1 highlights large variations in the previously reported energetic landscapes for the ring opening and closing steps (4 → 5 and 5 → 6). Compared with the present QM/MM calculations, the early PM3 studies^{23,24} returned a similar overall exothermicity for converting 4 to 6 but place the intermediate 5 and the activation barrier leading from 4 → 5 ~20 kJ mol⁻¹ higher in energy. Kang and Musgrave¹³ reported an *E_a* value for step 4 → 5 similar to that returned by the present QM/MM calculations, but the relaxed steric constraints associated with their cluster model implied too great a stability for 5. Like Kang and Musgrave,¹³ we find a large (>200 kJ mol⁻¹) barrier for the direct insertion process 4 → 6. This is in marked contradiction with the study of Oleinik et al.,¹⁵ which has 5 as a TS (with an *E_a*, defined relative to the radical intermediate 4, of only 54.4 kJ mol⁻¹). The latter calculations also underestimate the exothermicity of CH₂ incorporation within the lattice (i.e., of converting 4 to 6) by a factor of ~2; the implicit underestimation of the barrier to the reverse (ring-opening) process suggests that diamond {100} etching efficiencies are likely to have been overestimated in the KMC modeling of Battaile et al.¹² The MRMP2 (QM/MM) calculations of Tamura and Gordon¹⁶ find the overall conversion from 4 to 6 to be almost thermoneutral but with activation barriers comparable to those of our work.

B. Dimer Trough Bridging Mechanism. This derives from the HH mechanism proposed by Harris¹⁷ and subsequently modified by Harris and Goodwin.⁴⁵ It involves incorporation of a bridging methylene group across the trough between successive C–C dimers in a chain and, as Figure 3 shows, could occur by two possible mechanisms: a diradical pathway via intermediate 13 or a sterically hindered sequence of abstraction and addition reactions (8 → 12). The version of the latter mechanism described here is a modification of the original

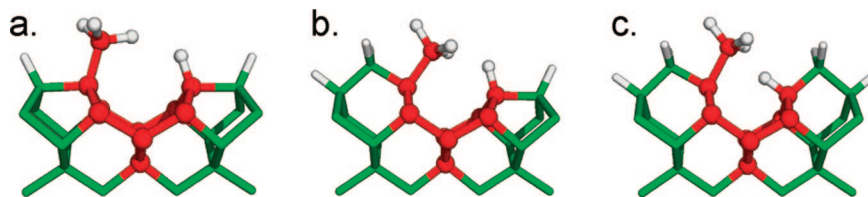


Figure 4. The three environments used when modeling the dimer trough bridging mechanism for carbon incorporation on a 2×1 reconstructed, H-terminated diamond (100) surface: (a) nucleation, (b) propagation, (c) termination step. The displayed structures correspond to three variants of structure **9** in Figure 3, with the QM region highlighted in red.

TABLE 3: Calculated (QM/MM, 6-311G Basis Set) Energy Changes, ΔE , and Activation Energies, E_a , (Both in kJ mol^{-1}) Associated with the Various Elementary Steps Involved in CH_2 Incorporation across the Trough between Successive Dimers in a Chain As Depicted in Figure 3, for Three Local Variants of **9** with Small QM Regions As Defined in Figure 4 and the Larger QM Region in the Case of the One Neighboring Inclusion As Shown in Figure 3^a**

	pristine surface (— · —) [Figure 4a]		1 neighboring inclusion (∧ · —) [Figure 4b]			2 neighboring inclusions (∧ · ∧) [Figure 4c]	
	small QM	PM3	small QM	large QM	PM3	small QM	PM3
	Steric Route						
8 → 9	−389.7	−312.5	−245.6	−219.1	−101.3	−149.3	45.6
TS		0.0		0.0	61.9		101.3
9 → 10	−21.1	43.5	−67.9	−67.7		−114.4	
TS				31.1			
10 → 11	8.5	43.5	6.3	5.7		−12.5	
TS		81.2		20.0			
	Diradical						
8 → 13	4.1		5.2	−7.2		−5.1	
TS				6.2			
13 → 11	−406.4	−315.5	−312.5	−274.0	−195.8	−271.1	−129.3
TS		0.0		0.0	10.0		36.0
	Ring Closing						
11 → 12	−113.1		−377.3	−369.1		−516.7	

^a The columns headed PM3 show the corresponding energies reported in ref 24.

trough bridging mechanism¹⁷ that avoids a sterically unfavorable H-atom abstraction from the diamond surface (the direct step from **9** → **11** in Figure 3, for which we calculate $E_a = 39.4 \text{ kJ mol}^{-1}$) by, instead, invoking a surface rearrangement process in which an H atom migrates from the surface to the pendant CH_2 radical (step **10** → **11** in Figure 3). H abstraction from the resulting surface bound CH_3 group is then followed by ring closure (**11** → **12**).

In this section, we explore the trough bridging mechanism as a possible means of nucleating (Figure 4a), propagating (Figure 4b), and as a terminating step (Figure 4c) in growth on a diamond {100} surface. The QM/MM model was modified so that the QM region spanned the trough between successive C–C dimers in a chain as illustrated in Figure 4. The starting species was chosen to be the surface radical site, as this can be created during the ring opening/closing incorporation mechanism. The sterically hindered pathway for incorporation across the dimer trough starts with formation of a C–C bond, with the incident CH_3 competing for space with an H atom bonded to the neighboring dimer (step **8** → **9** in Figure 3). The surface environment in the immediate vicinity of the pendant CH_3 group and the surface H atom determines their relative proximity, their competition for space, and the strength of the resulting C–C bond to the pendant CH_3 group. As Table 3 shows, the bond strength calculated by using a QM region as illustrated in Figure 4 ranges from strong ($\Delta E = -389.7 \text{ kJ mol}^{-1}$), in the case when the CH_3 group adds to a pristine surface (Figure 4a), to weak ($\Delta E = -149.3 \text{ kJ mol}^{-1}$), when the CH_3 adds to a trough between two surface dimers that have already been expanded by incorporating CH_2 groups (e.g. by the ring opening/closing mechanism, Figure 4c).

Further tests were carried out to check the sensitivity of these calculations to the detailed choice of QM region.⁴¹ By way of illustration, the energy differences marked on Figure 3 were obtained for the one neighboring inclusion case but by using a slightly larger QM region (i.e., that shown in Figure 4b with, in addition, the C atom in the adjoining dimer and the two C atoms in the inserted dimer as illustrated in the inset to Figure 3). The most obvious consequence of extending the QM region in this way is to allow the radical sites in the appropriate forms of **8** and **13** to be correctly modeled as tertiary carbons; this manifests itself as a modest reduction in the strengths of the C–C bonds formed in steps **8** → **9** and **13** → **11**.

The trend in C–C bond strength as the number of neighboring inserting CH_2 groups increases mimics that found with the earlier PM3 calculations, although, again, the C–C bond strengths returned by the QM/MM calculations are in each case larger. Furthermore, the present calculations find CH_3 addition to any radical site on the {100} surface to be a barrierless process, in contradiction to conclusions reached in the earlier PM3 calculations.²⁴ It is not entirely clear why barriers were found in the earlier work. One possibility is that a restricted ansatz was used to describe the singlet PES corresponding to the approaching pair of radicals. At short-range, this is appropriate, but at the longer range relevant for the addition step, an unrestricted ansatz allowing the two unpaired electrons to uncouple is more appropriate. Our B3LYP QM/MM calculations use an unrestricted ansatz to describe the open-shell singlet wave function in this region, and we find a smooth energy curve with no barrier. Although the unrestricted B3LYP calculations are by no means exact, they are sufficiently accurate for us to be confident that there will be no energy barrier for these steps.

The present study thus suggests that the rate of CH₃ addition to a radical site on the {100} surface is relatively independent of the local environment, although the stability of this adduct and its resistance to subsequent loss certainly is not.

Attention now switches to the possible surface rearrangement reactions involving the pendant CH₃ group and the surface bound H atom (steps **9** → **11** in Figure 3). Formation of the pendant CH₂ radical, by H-atom abstraction from the sterically restricted CH₃ group (step **9** → **10** in Figure 3), becomes progressively more exothermic if one, or both, of the neighboring dimers have already incorporated a bridging CH₂ group ($\Delta E = -21.1$, -67.9 kJ, and -114.4 kJ mol⁻¹ for the structures displayed in Figure 4a,b,c, respectively), as the induced geometry changes reduce the steric interactions across the dimer trough. H migration across the dimer trough from the diamond surface to the pendant CH₂ group (step **10** → **11** in Figure 3) is essentially thermoneutral in all three scenarios (Table 3). As Table 3 shows, the earlier PM3 studies²⁴ found this process to be mildly endothermic (on the pristine {100} surface) and to have an activation barrier four times larger than that found in the present calculations. However, the energetic changes suggested by the present work merely serve to reinforce the consensus view that the rate of equilibration between intermediates **10** and **11** will be much faster than the per-site rates of H abstraction or H addition under typical CVD conditions (see later).

Figure 3 also illustrates an alternative route to **11**, involving a second H abstraction from the precursor **8**, forming the diradical **13** (modeled here as a spin-triplet species with two unpaired electrons), followed by addition of a CH₃ radical. The diradical formation step (**8** → **13**) is calculated to be roughly thermoneutral. Subsequent addition of a CH₃ radical to **13** is more exothermic than the corresponding addition to the single radical site **8**, because of reduced steric interaction with the neighboring dimer chain. Once again, as Table 3 shows, these trends in C–C bond strength with change in local structure parallel those found in the PM3 study,²⁴ but the QM/MM calculations again return consistently greater bond strengths and find no evidence for any barrier to C–C bond formation.

Both pathways from starting species **8** involve two gas-surface reactions (an H abstraction and a CH₃ radical addition) and result in a common intermediate (**11**) that is then stabilized by the same ring-closing reaction (step **11** → **12** in Figure 3) that is instigated by a further H-abstraction reaction. This reaction presumably has a small reaction barrier associated with the hydrogen atom abstraction, but description of this barrier with B3LYP is difficult, and we have not explicitly located the barrier. The abstraction leads to a diradical that can exist in either a triplet or a singlet state. There will certainly be no barrier to C–C bond formation on the singlet surface; therefore, conversion to **12** will occur in a single step. The triplet diradical will be able to convert to the singlet quickly (as discussed below in more detail for related processes) so that whichever spin state is involved, the net effect of hydrogen atom abstraction will be rapid formation of **12**. In marked contrast to the previous steps, the energetics for this final ring-closing step become progressively more favorable in the case when one, or both, of the neighbor C–C dimer bonds have undergone prior CH₂ incorporation, because this reduces the distance between the ring closing C atoms. In the case of an otherwise pristine diamond surface (Figure 4a), the distance between the C atom of a pendant CH₃ group and the C atom of a surface radical (2.68 Å) together with the large separation between the dimer rows (3.46 Å) results in a highly strained ring-closed species, which

manifests itself as a small reaction exothermicity ($\Delta E = -113.1$ kJ mol⁻¹); the resulting C–C bonds in this case are too weak for structure **12** to constitute a stable, terminating structure. Species **12** in this case is identical to structure **23**, an intermediate in the carbon migration mechanism discussed below and, as mentioned in that context, will ring open and rearrange to give a species corresponding to insertion into one of the neighboring reconstructions. The corresponding distances in the other extreme, where CH₂ groups have inserted into both of the neighboring dimer bonds (Figure 4c), are 2.50 and 2.90 Å. Ring closure in this case is highly favorable ($\Delta E = -516.7$ kJ mol⁻¹), reflecting the consequent relief of strain and steric hindrance.

Sections through PESs such as those shown in Figures 1 and 3 provide necessary, but not sufficient, input for discussion of the stabilities of the various intermediates and likely reaction probabilities. The key quantity determining reaction rates and equilibria is the free energy. Diamond CVD processes typically span the temperature range 1000–1400 K. In fact, the concentration of gas-phase H atoms is higher than suggested by this temperature, because they are produced in much hotter regions by the filament or microwave discharge, and the subsequent recombination of two gas-phase H atoms to form H₂ is slow. Entropic effects will make a significant contribution to the free energy profile at these temperatures, particularly in steps that involve loss or production of a gas-phase species. By way of illustration, a step such as **8** → **9** or **13** → **11** in Figure 3, where a gas-phase CH₃ species is accommodated at the surface, will have an associated $\Delta_p S$ of about -100 J mol⁻¹ K⁻¹. The entropic contribution, $T\Delta_p S$, will thus be ~ 120 kJ mol⁻¹ at typical CVD growth temperatures and sufficient to render formation of weaker C–C bonds improbable. From Table 3, we therefore conclude that the nucleation step **8** → **9** must be very improbable when the trough of interest is between two previous incorporations (Figure 4c) and that any trough bridging in such cases will occur via the diradical mechanism **8** → **13**. The fraction of radical sites on the diamond {100} surface depends on the substrate temperature and the incident H-atom flux but is generally considered to be in the range 0.05–0.1 under typical CVD conditions.²⁸ The fraction of diradical species such as **13**, which require H-atom abstraction reactions at two adjacent C atoms, must be lower, that is, ~ 0.0025 – 0.01 .

On these bases, the best compromise site for carbon incorporation via the trough bridging mechanism is addition to a site with a previous incorporation adjacent to one reconstructed dimer (Figure 4b). This structural arrangement presents less steric constraint to the initial CH₃ adsorption than in the case when both neighboring dimers have undergone CH₂ insertion but also exhibits a sufficiently small separation (3.19 Å) between the dimer rows to encourage formation of the terminating C–C bond in **12**. Both the single and diradical pathways are feasible routes for incorporation of methyl, as both require identical numbers of gas-phase reactions with similar activation energy profiles. Reference to Table 3 highlights the increasing strength of the C–C bond formed in step **13** → **11** (relative to that formed in the corresponding step **8** → **9**) when the participating dimers have already expanded via the ring opening/closing mechanism, suggesting an increased contribution for the diradical pathway in these cases. This suggests that trough bridging should be able to occur at both sides of a CH₂ group in a reconstructed dimer bond, though the energetics do not appear to be such that this process would be kinetically favored over CH₂ incorporation into a remote dimer reconstruction.

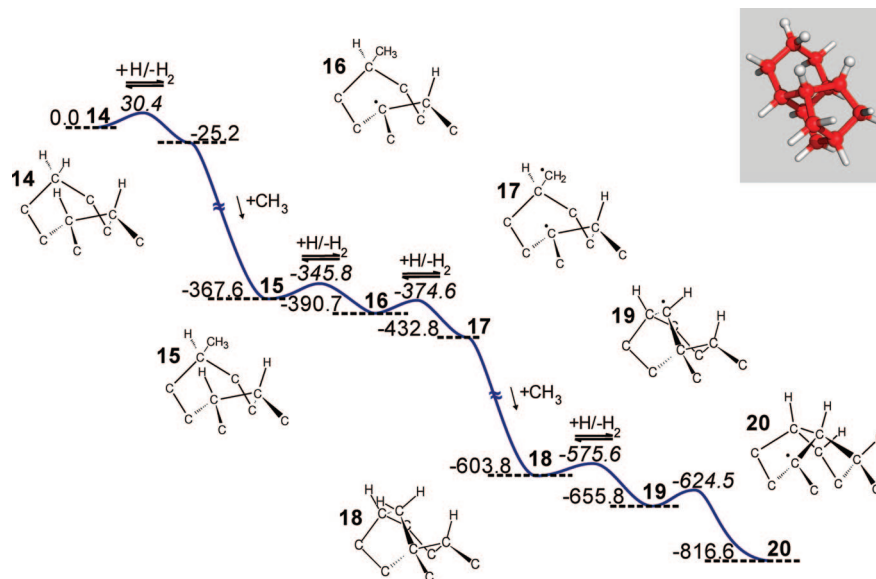


Figure 5. PES illustrating the way in which CH_3 radical addition can lead to nucleation of a new reconstructed dimer layer on the diamond {100} surface. Optimised structures of the intermediates returned by the QM/MM calculations are illustrated, with the QM region used in these calculations shown in the top right-hand corner. Energies (B3LYP QM/MM, 6-311G** basis set) are quoted in units of kJ mol^{-1} , relative to that of structure 14.

C. Generation of a Dimer Reconstruction. Mechanisms for creating a C–C dimer on a reconstructed diamond {100} surface under CVD conditions have received relatively little attention thus far. Figure 5 illustrates a plausible dimer formation mechanism, which involves CH_3 addition to a previously incorporated C atom, followed by a reconstruction with a neighboring C–C dimer. The mechanism proceeds by formation of a bridge between the inserted dimer and an adjacent dimer in the same row by using the pendant methyl group which, upon H abstraction, incorporates into the pre-existing dimer, forming a new C–C dimer at 90° to the precursor dimer bonds. Such nucleation of a new row can be viewed as a step formation mechanism. In its outcome, at least, it is somewhat analogous to a proposed pathway for incorporating a migrated $\text{C}=\text{CH}_2$ group following adsorption of acetylene.⁴⁶

The model shown in Figure 1 was modified for these QM/MM calculations so that the MM surface region included a chain of dimers each with an inserted CH_2 group adjacent to and parallel with the C–C dimer bond in the base QM cluster. The QM region itself was modeled by the cluster from Figure 1 but expanded to include the appropriate section of the inserted chain, as illustrated by **14** in Figure 5. As before, formation of the pendant CH_3 group on a previously incorporated C atom (step **14** \rightarrow **15** in Figure 5) proceeds via successive H abstraction and CH_3 addition reactions. Abstraction of one H atom requires activation ($E_a = 30.4 \text{ kJ mol}^{-1}$) but is exothermic ($\Delta E = -25.2 \text{ kJ mol}^{-1}$); the C–C bond formation step is barrierless, and highly exothermic ($\Delta E = -342.3 \text{ kJ mol}^{-1}$). Formation of the bridging CH_2 group (step **15** \rightarrow **18** in Figure 5) involves two H-atom abstraction processes and is analogous to steps **10** \rightarrow **12** in the sterically hindered form of the trough bridging mechanism (Figure 3).

As in the sterically hindered version of the trough bridging sequence (Section B), these H-abstraction reactions could occur in more than one sequence. The lowest energy pathway for sequence **15** \rightarrow **18** involves an initial H abstraction from either of the two C atoms in the adjacent reconstructed C–C dimer ($E = -23.1 \text{ kJ mol}^{-1}$, $E_a = 21.8 \text{ kJ mol}^{-1}$), followed by an H abstraction from the pendant CH_3 group ($\Delta E = -42.1 \text{ kJ mol}^{-1}$, $E_a = 16.1 \text{ kJ mol}^{-1}$) and subsequent ring closure. The second

abstraction leads to a diradical, which is expected to be formed in a $\sim 1:3$ mixture of singlet and triplet states. The species shown in Figure 5 is the triplet state, which can be located as a local minimum, because it cannot undergo ring closure with C–C bond formation to form **18**, which is a singlet. We have also attempted to optimize the geometry of the open-shell singlet diradical by using unrestricted B3LYP calculations. At the optimized geometry of the triplet state, the singlet and triplet states lie very close in energy, but optimization leads directly to **18** without an energy barrier.

How fast is the ring closure of the triplet state to form **18** likely to be? Rates of spin-forbidden reactions are known⁴⁷ to depend on two factors: the energy required to reach the seam of crossing between the two PESs involved and the probability of surface crossing in the vicinity of the seam, which depends on the strength of the coupling between the two electronic states. Given the near-degeneracy of the triplet and singlet states at the optimized geometry of the triplet, the seam of crossing is expected to lie close to the triplet minimum, and thermal motion will enable the triplet state to reach the crossing seam with the singlet at almost every vibrational period ($\sim 100 \text{ fs}$). Spin–orbit coupling between the singlet and triplet states of hydrocarbon diradicals is typically rather weak,⁴⁸ but together with spin–spin coupling, it should still be enough to promote spin-state change in at least one seam crossing event per 10^4 . Hence, the ring closure to form **18** on the triplet surface is expected to occur on the nanosecond time scale or faster.

The initial H abstraction, which was unfavorable in the trough bridging mechanism ($E_a = 31.1 \text{ kJ mol}^{-1}$ for the **9** \rightarrow **11** abstraction process, Figure 3), is less restricted in this present case because of the larger separation between the CH_3 group and the H atom which enables a more orthodox TS geometry and thus a lower activation energy. The alternative sequence, starting with an H abstraction from the pendant CH_3 , followed by migration of an H atom across the trough, a second H abstraction from the reformed CH_3 and eventual ring closure (i.e. the analogue of steps **8** \rightarrow **12** via **10** in Figure 3) is improbable in view of the high activation barrier calculated for the endothermic H migration step ($\Delta E = 7.5 \text{ kJ mol}^{-1}$, $E_a =$

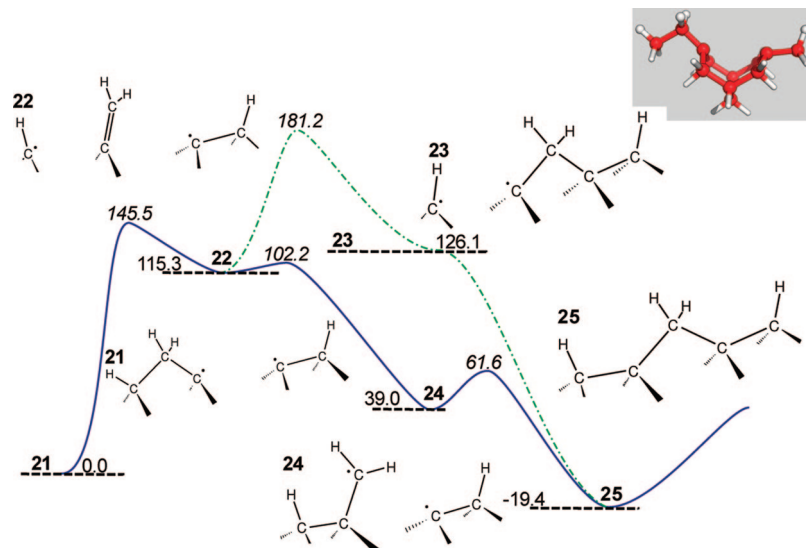


Figure 6. PES describing migration of a CH_2 group along a dimer chain on the 2×1 reconstructed, H-terminated diamond (100) surface. Optimised structures of the intermediates returned by the QM/MM calculations are shown, with the QM region used in these calculations shown in the top right-hand corner. Energies (B3LYP QM/MM, 6-311G** basis set) are quoted in units of kJ mol^{-1} , relative to that of structure **21**.

89.0 kJ mol^{-1}). This barrier arises from the large distance between the pendant CH_2 group and the surface H atoms.

The geometry of the bridging methylene group in **18** is such that, following one further and energetically feasible H-abstraction step ($\Delta E = -52.0 \text{ kJ mol}^{-1}$, $E_a = 28.1 \text{ kJ mol}^{-1}$), the resulting radical can insert directly into the reconstructed dimer (step **19** \rightarrow **20** in Figure 5) to form a reconstructed dimer at 90° to the initial pattern. The calculated exothermicity and activation barrier for this step are $\Delta E = -160.8 \text{ kJ mol}^{-1}$ and $E_a = 31.3 \text{ kJ mol}^{-1}$, respectively. The insertion step in this case differs from the normal ring opening/closing process (step **4** \rightarrow **6** in Figure 2) because the bridging C–C bond restricts the motion of the inserting radical, holding it in a favorable position for the direct insertion process.

A similar process is also possible in which addition of the new carbon atom occurs not to the inserted carbon atom but to the adjacent reconstructed dimer. A sequence of hydrogen atom abstractions similar to those outlined above can then lead to the same intermediate **18**. We have not explored this alternative process, but it is expected to be broadly comparable to the one described in Figure 5. Either way, it is clear that once one carbon atom has inserted into a reconstruction, there is a possible pathway leading to eventual formation of a new reconstruction on the next layer, by addition of an additional carbon and insertion into the reconstruction adjacent along the row of dimers. As mentioned above for the trough bridging mechanism, however, this process is not kinetically favored over insertion of carbon into a remote reconstruction. Hence, neither process can account for the observed tendency for the [100] surface to form large flat terraces.

D. Surface Carbon Migration Reactions. The results reported in the previous sections suggest that there are many different surface radical sites to which a gaseous CH_3 radical can add, but that some of the strongest C–C bonds are formed in the case of addition to a single radical site on a locally pristine diamond surface. Given that it is likely that there are many such sites available under standard CVD conditions, it might be expected that CH_3 adsorption and subsequent incorporation would tend to occur at random sites on the growing diamond surface. Thus, we have also reinvestigated previous proposals²⁶ that carbon species can migrate across the {100} surface,

offering a means for individual carbon species to coalesce and, possibly, form the locally smooth terraces, with organized rows of reconstructed dimers, revealed by surface science studies.^{7–9} We note, however, that the most thorough KMC calculations of growth on diamond {100} yet reported²⁷ speculate that this apparent ordering during growth might actually be the result of surface etching, postgrowth, during the time taken to switch off the CVD process and return the sample to room temperature.

Before considering the possibility of surface migration of carbon species, attention briefly switches to the feasibility of the migration of atomic hydrogen to a neighboring radical site upon a {100} diamond surface. The present QM/MM calculations reinforce the view that H-atom migration across a pristine diamond surface to a dimer radical site is an unlikely process. Our brief investigations focused upon the feasibility of atomic H migration to a surface radical site across a dimer trough and along a dimer row. These calculations were performed upon a pristine surface QM/MM model with QM regions of shape and size similar to those of **8** (Figure 3) and **26** (Figure 7, see later) for the two migration directions. Atomic hydrogen migration is deduced not to occur in either scenario because of the large activation barriers ($E_a = 301.3 \text{ kJ mol}^{-1}$, $320.6 \text{ kJ mol}^{-1}$, respectively).

In contrast, H-atom migration is energetically feasible in other cases, for example, from a neighboring preinserted C–C dimer or from an adjacent pendant CH_3 group as in step **10** \rightarrow **11**. Overall, though, the most facile process for migration of a radical site on a pristine surface is likely to be the same gas-phase H-abstraction/addition reaction sequence that underpins CH_3 incorporation.

Figure 6 illustrates the previously proposed mechanism²⁶ by which a CH_2 group might migrate along a dimer chain on the H-terminated, 2×1 reconstructed diamond {100} surface. The sequence starts from structure **21** (the analogue of structure **6** in Figure 1), with a CH_2 group incorporated in a C–C dimer bond, adjacent to a radical site. This starting species involves two radicals and is treated here as a spin triplet. Ring opening results in an unsaturated pendant CH_2 group with a radical site on either side (structure **22** in Figure 6). This intermediate can revert to structure **21** (a null process). However, it can also reform the reconstructed dimer **24** over a low barrier, whereby

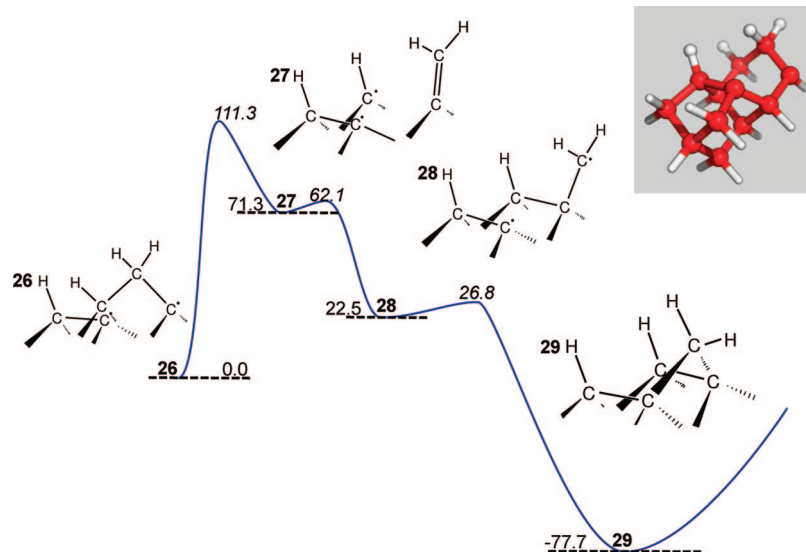


Figure 7. PES describing migration of a CH_2 group on the 2×1 reconstructed, H-terminated diamond (100) surface. Optimised structures of the intermediates returned by the QM/MM calculations are shown, with the QM region used in these calculations shown in the top right-hand corner. Energies (B3LYP QM/MM, 6-311G** basis set) are quoted in units of kJ mol^{-1} , relative to that of structure **26**.

the unsaturated pendant CH_2 group gives up a π electron and becomes a pendant methylene radical. This step has a positive activation energy of 2.3 kJ mol^{-1} at the level of theory used for geometry optimization (QM/MM with B3LYP/6-31G*); on the basis of the single-point energies calculated by using the larger 6-311G** basis set, however, the TS is predicted to lie several kJ mol^{-1} lower than **22**. This suggests either that there is in reality no barrier to this step or that it is very small indeed. Diradical **24** can then ring close exothermically to form the strained intermediate **25**.

The singlet and triplet surfaces are near-degenerate for **21**, **22**, and **24**. For example, we calculate that the singlet state of **24** (treated as an open-shell singlet species with two unpaired electrons obtained by using unrestricted B3LYP) lies at a relative energy of 30.5 kJ mol^{-1} , compared to **21**, whereas the corresponding triplet state of **24**, shown in Figure 6, lies at a relative energy of 39.0 kJ mol^{-1} . The optimum geometries on the two PESs are also very similar. Hydrogen-atom abstraction, yielding **21**, is expected to give a $\sim 1:3$ mixture of singlet and triplet states, and this ratio should be maintained for **24**. Ring closure to **25** can only occur on the singlet surface. As discussed above for a similar process, however, triplet **24** should be able to convert to the singlet on the nanosecond (or faster) time scale. Note that, unlike some of the other C–C bond formation reactions described in this work, the singlet ring formation step involves a small energy barrier of 22.6 kJ mol^{-1} relative to the triplet minimum of **24** because of the need to rotate the pendant CH_2 group before bonding can occur.

A higher energy route to intermediate **25**, involving trough bridging (intermediate **23**) before dimer reformation, has been identified also. Intermediate **23** is stable on the triplet PES, but geometry optimization on the singlet surface leads directly to **25** without a barrier. Structure **25** is too strained to be a stable long-lived intermediate; it can open in two ways, either reverting to **21** or leading on to the migrated species (**21a**).

Figure 7 depicts the calculated energy landscape for migration along the orthogonal surface coordinate, across the trough between dimers in neighboring chains (i.e. along a row). Here, we require a CH_2 group incorporated in a C–C dimer bond and a single radical site on the next dimer in the row (structure **26** in Figure 7). The initial ring opening step is again found to

present the highest energy barrier on the minimum energy pathway, and again, the resulting intermediate (**27**) comprises an unsaturated pendant CH_2 group with two adjacent radical sites. The next step leading to migration in this case is reformation of a dimer bond in the first chain (step **27** \rightarrow **28**, again this has a low activation energy of 5.6 kJ mol^{-1} at the B3LYP/6-31G* QM/MM level, but the TS is predicted to be more stable than **27** when using the larger 6-311G** basis set). This is followed by ring closure forming intermediate **29**, which in this case includes a four-membered cyclobutane ring and is thereby also highly strained and, upon ring-opening, will either revert to **26** or complete the migratory sequence to form structure **26a**. As in the case of migration along the dimer chain, most of the species in this pathway (**26**, **27**, and **28**) are diradicals that are again found to have near-degenerate singlet and triplet states. The intermediate **29** must however exist as a singlet; therefore, spin-state change may need to occur before ring closure. As discussed above, this should occur rapidly if needed.

The energetics displayed in Figures 6 and 7 need to be interpreted with due caution. The strained intermediates **25** (and **29**) are both calculated to lie at a lower total energy than the starting species **21** (and **26**) and might therefore be expected to accumulate on the surface during the CVD process. Indeed, on the basis of present energy calculations, **25** and **29** are predicted to be more abundant than **21** and **26**. The latter, however, are present in relatively low concentration compared to the corresponding H-terminated analogues, and these should dominate over **25** and **29** also.

Table 4 compares the QM/MM calculated energies for both migration sequences with results from the earlier PM3 calculations.²⁶ The two data sets are very comparable up to the point of dimer reformation in both the along-chain and along-row migration pathways (i.e., until reaching the respective structures **24** and **28**, with their pendant methylene radical groups). Both return similar activation barriers for the initial ring opening steps (**21** \rightarrow **22** and **26** \rightarrow **27**) and suggest that the next step, reformation of the C–C dimer bond to give intermediates **24** and **28**, evolves over a low barrier. Both also predict that species **24** and **28** lie $\sim 20\text{--}40 \text{ kJ mol}^{-1}$ above the respective starting structures. The two methods diverge however in describing the energy required to reach the bridged species **25** and **29**. Our

TABLE 4: Calculated (QM/MM, 6-311G Basis Set) Energy Changes, ΔE , and Activation Energies, E_a , (Both in kJ mol^{-1}) for the Various Elementary Steps Involved in CH_2 Migration along a Dimer Chain (as in Figure 6) and along a Dimer Row (as in Figure 7)^a**

	migration along a dimer chain (Figure 6)		migration along a dimer row (Figure 7)		
	QM/MM	PM3	QM/MM	PM3	PM3
$\Delta E_{21 \rightarrow 22}$	115.3	100.4	$\Delta E_{26 \rightarrow 27}$	71.3	99.6
E_a	145.5	151.9	E_a	111.3	151.9
$\Delta E_{22 \rightarrow 24}$	-76.3	-51.8	$\Delta E_{27 \rightarrow 28}$	-48.8	-51.8
E_a	-13.1	12.1	E_a	-9.2	12.1
$\Delta E_{24 \rightarrow 25}$	-58.6	3.8	$\Delta E_{28 \rightarrow 29}$	-100.2	14.2
E_a	22.6	111.3	E_a	4.3	125.5
$\Delta E_{22 \rightarrow 23}$	10.8	-56.1			
E_a	65.9	62.3			
$\Delta E_{23 \rightarrow 24}$	-145.5	8.0			
E_a	0	46.0			

^a Values in columns headed PM3 are from ref 26.

QM/MM calculations predict that this step is exothermic and occurs easily, especially when the diradical starts on the singlet PES, when only a small barrier needs to be crossed. When the diradicals start out as triplet species (as they should do in roughly three cases out of four, because of the near degeneracy of the singlet and triplet states), a spin-state change is needed, but this should be facile also. Hence, the rate-limiting step for the whole migration event is the initial ring opening from **21** or from **26**.

In contrast, the PM3 calculations²⁶ predict steps **24** \rightarrow **25** and **28** \rightarrow **29** to be endothermic and to involve high barriers. The PM3 results match the present findings in as much that the initial ring opening steps (**21** \rightarrow **22** and **26** \rightarrow **27**) are predicted to have the largest E_a values. However, intermediates **24** and **28** are both higher in energy than the starting diradicals, and the PM3 calculations predict that the highest energy TSs relative to **21** and **26** are those for the ring-closure steps (though the difference in energy with respect to the ring-opening TSs is small). The net calculated energy barriers are also higher than those in the present work, at 159.9 and 173.3 kJ mol^{-1} , respectively, (cf the corresponding B3LYP barriers of 145.5 and 111.3 kJ mol^{-1}). The intermediates **25** and **29** also have different predicted properties in the two sets of calculations. The DFT calculations show them to be more stable in energy terms than the starting diradicals (although as noted above the hydrogenated species should be even more stable), whereas the PM3 calculations predict that they should be somewhat less stable than the starting diradicals.

How can one account for these differences, and which result is correct? The second trend, of higher stability of the intermediates in the B3LYP QM/MM calculations, is due to the fact (already noted above when discussing addition of CH_3 to radical sites on the surface) that PM3 appears to underestimate the C–C bond energies. Our calibration calculations suggest that B3LYP reproduces this key energetic aspect quite accurately. The first trend, of a higher barrier in the PM3 calculations, also mirrors the observation found earlier for CH_3 addition to radical sites. In many cases, PM3 led to barriers for these steps where none could be found at the B3LYP QM/MM level. We suggested that this might be due to the use of a restricted ansatz to describe the electronic structure for the diradical; we found that an unrestricted approach was needed to describe this part of the PES in a meaningful way.

Despite these differences, both approaches lead to the same overall prediction, namely, that there are plausible migration

routes for both along-chain and along-row migration of CH_2 groups. In fact, compared to the earlier study,²⁶ the slightly lower overall barrier obtained here means that the rate constants for these migration processes may even be slightly higher than the values predicted by Frenklach and Skokov ($\sim 10^8 \text{ s}^{-1}$ at 1200 K). Migration of carbon insertions will ultimately lead to modified steps in which one insertion meets another. In such cases, modified forms of the trough bridging or dimer reconstruction generation processes described above can be formulated, that lead to extension of the appropriate sections of the new diamond layer. These mechanisms have not been explored here, because they are closely analogous to the steps already described.

IV. Conclusions

A number of key reaction sequences by which carbon incorporates into the diamond {100} surface under representative CVD conditions have been reinvestigated by using QM/MM methods, with the QM region treated at an accurate level of theory (B3LYP with a 6-31G* basis set for geometry optimization, with single points calculated by using a 6-311G** basis set). Previous studies of some of these reactions either were conducted by using QM/MM methods with a much less accurate QM method (semiempirical PM3 theory) or used QM methods only on small cluster models and hence could not address the effects of the surface environment. Although many of the trends predicted by the present work were mentioned in previous studies, a number of significant differences are noted, especially with respect to the very thorough PM3 work of Frenklach et al.^{20–27} The systematic nature of the present work also provides additional insight, especially compared to some of the previous higher-level QM studies that only address a limited number of steps.^{13,14,16} Finally, several of the mechanisms considered involve diradical species that could in principle exist as either singlet or triplet species. Unlike previous studies, the present work addresses the spin-forbidden interconversions between these states and shows that triplet species can convert to singlets fast enough that this process does not represent a bottleneck in the overall growth of CVD diamond.

The key difference of the present B3LYP QM/MM PESs with respect to those obtained in the influential PM3 studies of Frenklach et al.^{22–27} is that C–C bond formation steps, either between gas-phase CH_3 and surface radicals or between two surface radicals, are predicted to be more exothermic and to involve lower barriers. Hence, CH_3 radical addition is predicted to occur without an energy barrier for all diamond surface radical sites considered in this work. Also, bridged intermediates formed in carbon migration processes are predicted to be more stable and easier to reach than those in the earlier work, reinforcing the view that migrations can be relatively rapid under CVD conditions. For the initial step in growth on the [100] surface, the present QM/MM calculations also highlight some errors in the energies calculated at a variety of levels of theory by using QM calculations on small cluster mimics of the diamond {100} surface.^{13,15,16}

The overall mechanism for incorporation of carbon into a growing diamond {100} surface emerging from the present study involves the following steps, starting from (and returning to) a pristine, hydrogen-terminated and 2×1 reconstructed smooth surface. First, CH_3 undergoes insertion into a reconstructed dimer by the ring opening and closing mechanism. This process, as all the others discussed here,

occurs in a fairly large number of elementary steps, many of which involve either hydrogen-atom abstraction or hydrogen-atom addition, emphasizing the key role played by H atoms in diamond CVD. Diamond etching in the absence of gas-phase carbon species under CVD conditions cannot be accounted for by simple reversal of the insertion process, because the key C–C bond formation step is highly exothermic and hence effectively irreversible, even at high temperature. The most likely sequence of reactions leading to carbon loss is instead predicted to involve addition of a second methyl group to a pendant CH₂ radical site on the surface, followed by H atom abstraction and ethene loss.

This carbon incorporation process needs to be complemented by others to lead to growth of a complete new surface layer. The present calculations suggest that a carbon atom can be added to the trough between two reconstructions in a dimer row through a bridging mechanism. This process is not expected to be particularly favorable, however (e.g., no more so than insertion into a remote site on the surface), so that insertion of a single carbon atom into a dimer does not of itself trigger facile growth of a whole new layer of CVD diamond. Our calculations also show that a modified form of the insertion mechanism can lead to insertion of CH₃ into a reconstruction neighboring a reconstruction into which insertion has already occurred, with simultaneous formation of a reconstruction on the next diamond layer. Again, the process can occur but is not more favorable than a normal insertion process; therefore, it is not expected to lead to a surface nucleation effect.

A key result is that carbon-atom migration steps, both along rows and chains of dimers, are predicted to occur with relatively low barriers. These processes, already characterized at lower levels of theory,²⁶ have been incorporated in KMC schemes of diamond growth and shown to play an important role in formation of smooth diamond surfaces.²⁷ Our calculations confirm relatively low barriers for these steps; in fact, slightly lower activation energies are predicted than those found previously. This confirms that carbon atom migration, apparently much more complex than adatom migration in simple models of crystal growth due to the complex pattern of bond breaking and formation that is required, can indeed occur during diamond CVD. Where migration leads to one carbon insertion joining with another, modifications of the dimer reconstruction regeneration mechanism mentioned above can be formulated, that lead to extension of the new diamond layer.

Acknowledgment. The authors are most grateful to EPSRC for funding via the pilot portfolio partnership LASER and for an Advanced Research Fellowship to J.N.H., to Element Six Ltd for studentship support (A.C.), and to Drs. J. E. Butler (Naval Research Laboratory, Washington, D.C.) and Yu. A. Mankelevich (Moscow State University) for numerous helpful discussions.

References and Notes

- (1) Brunet, F.; Germe, P.; Pernet, M.; Deneuville, A.; Gheeraert, E.; Mambou, J. *Diam. Rel. Mater.* **1997**, *6*, 774.
- (2) Yan, C. S.; Mao, H. K.; Li, W.; Qian, J.; Zhao, Y.; Hemley, R. J. *Phys. Status Solidi A* **2004**, *201*, R25.
- (3) Bogdan, G.; Nesládek, M.; D'Haen, J.; Maes, J.; Moshchalkov, V. V.; Haenen, K.; D'Olieslaeger, M. *Phys. Status Solidi A* **2005**, *202*, 2066.
- (4) Celi, F. G.; Butler, J. E. *Annu. Rev. Phys. Chem.* **1991**, *42*, 643.
- (5) Goodwin, D. G.; Butler, J. E. In *Handbook of Industrial Diamonds and Diamond Films*; Prelas, M. A., Popovici, G., Bigelow, L. G., Eds.; Marcel Dekker: New York, 1998; pp 527–81.

- (6) Ashfold, M. N. R.; May, P. W.; Petherbridge, J. R.; Rosser, K. N.; Smith, J. A.; Mankelevich, Y. A.; Suetin, N. V. *Phys. Chem. Chem. Phys.* **2001**, *3*, 3471.
- (7) Tsuno, T.; Tomikawa, T.; Shikata, S.; Imai, T.; Fujimori, N. *Appl. Phys. Lett.* **1994**, *64*, 572.
- (8) Nützenadel, C.; Küttel, O. M.; Diederich, L.; Maillard-Schaller, E.; Gröning, O.; Schlapbach, L. *Surf. Sci.* **1996**, *396*, L111.
- (9) Bobrov, K.; Mayne, A.; Comtet, G.; Dujardin, G.; Hellner, L.; Hoffman, A. *Phys. Rev. B* **2003**, *68*, 195416.
- (10) Garrison, B. J.; Dawnkaski, E. J.; Srivastava, D.; Brenner, D. W. *Science* **1992**, *255*, 835.
- (11) Kaukonen, M.; Sitch, P. K.; Jungnickel, G.; Nieminen, R. M.; Pöykkö, S.; Porezag, D.; Frauenheim, Th. *Phys. Rev. B* **1998**, *57*, 9965.
- (12) Battaile, C. C.; Srolovitz, D. J.; Oleinik, I. I.; Pettifor, D. G.; Sutton, A. P.; Harris, S. J.; Butler, J. E. *J. Chem. Phys.* **1999**, *111*, 4291.
- (13) Kang, J. K.; Musgrave, C. B. *J. Chem. Phys.* **2000**, *113*, 7582.
- (14) Tamura, H.; Zhou, H.; Hirano, Y.; Takami, S.; Kubo, M.; Belosludov, R. V.; Miyamoto, A.; Imamura, A.; Gamo, M. N.; Ando, T. *Phys. Rev. B* **2000**, *62*, 16995.
- (15) Oleinik, I. I.; Pettifor, D. G.; Sutton, A. P.; Butler, J. E. *Diam. Rel. Mater.* **2000**, *9*, 241.
- (16) Tamura, H.; Gordon, M. S. *Chem. Phys. Lett.* **2005**, *406*, 197.
- (17) Harris, S. J. *Appl. Phys. Lett.* **1990**, *56*, 2298.
- (18) Petrini, D.; Larsson, K. *J. Phys. Chem. C* **2007**, *111*, 795.
- (19) Van Regemorter, T.; Larsson, K. *J. Phys. Chem. A* **2008**, *112*, 5429.
- (20) Huang, D.; Frenklach, M.; Maroncelli, M. *J. Phys. Chem.* **1988**, *92*, 6379.
- (21) Huang, D.; Frenklach, M. *J. Phys. Chem.* **1991**, *95*, 3692.
- (22) Frenklach, M.; Wang, H. *Phys. Rev. B* **1991**, *43*, 1520.
- (23) Skokov, S.; Weiner, B.; Frenklach, M. *J. Phys. Chem.* **1994**, *98*, 8.
- (24) Skokov, S.; Weiner, B.; Frenklach, M. *J. Phys. Chem.* **1994**, *98*, 7073.
- (25) Skokov, S.; Weiner, B.; Frenklach, M. *J. Phys. Chem.* **1995**, *99*, 5616.
- (26) Frenklach, M.; Skokov, S. *J. Phys. Chem. B* **1997**, *101*, 3025.
- (27) Netto, A.; Frenklach, M. *Diam. Rel. Mater.* **2005**, *14*, 1630.
- (28) Butler, J. E.; Woodin, R. L. *Phil. Trans. R. Soc. London A* **1993**, *342*, 209, and references therein.
- (29) Coltrin, M. E.; Dandy, D. S. *J. Appl. Phys.* **1993**, *74*, 5803.
- (30) Cheesman, A.; Harvey, J. N.; Ashfold, M. N. R. *Phys. Chem. Chem. Phys.* **2005**, *7*, 1121.
- (31) Field, M. J.; Bash, P. A.; Karplus, M. *J. Comput. Chem.* **1990**, *11*, 700.
- (32) Allinger, M. L. *J. Am. Chem. Soc.* **1977**, *99*, 8127.
- (33) Harvey, J. N. *Faraday Discuss.* **2004**, *127*, 165.
- (34) Tspis, A. C.; Orpen, A. G.; Harvey, J. N. *Dalton Trans.* **2005**, 2849.
- (35) *Jaguar*; Schrödinger Inc.: Portland, 2000.
- (36) Ponder, J. W. *TINKER: Software Tools for Molecular Design*, v4.0; Saint Louis, 2003.
- (37) Grimme, S. *J. Chem. Phys.* **2003**, *118*, 9095.
- (38) See e.g. (a) Halgren, T. A.; Lipscomb, W. N. *Chem. Phys. Lett.* **1977**, *49*, 225. (b) Xie, L.; Liu, H.; Yang, W. *J. Chem. Phys.* **2004**, *120*, 8039.
- (39) Frisch, M. J.; Trucks, G. W.; Schlegel, H. B.; Scuseria, G. E.; Robb, M. A.; Cheeseman, J. R.; Montgomery, J. A., Jr.; Vreven, T.; Kudin, K. N.; Burant, J. C.; Millam, J. M.; Iyengar, S. S.; Tomasi, J.; Barone, V.; Mennucci, B.; Cossi, M.; Scalmani, G.; Rega, N.; Petersson, G. A.; Nakatsuji, H.; Hada, M.; Ehara, M.; Toyota, K.; Fukuda, R.; Hasegawa, J.; Ishida, M.; Nakajima, T.; Honda, Y.; Kitao, O.; Nakai, H.; Klene, M.; Li, X.; Knox, J. E.; Hratchian, H. P.; Cross, J. B.; Bakken, V.; Adamo, C.; Jaramillo, J.; Gomperts, R.; Stratmann, R. E.; Yazyev, O.; Austin, A. J.; Cammi, R.; Pomelli, C.; Ochterski, J. W.; Ayala, P. Y.; Morokuma, K.; Voth, G. A.; Salvador, P.; Dannenberg, J. J.; Zakrzewski, V. G.; Dapprich, S.; Daniels, A. D.; Strain, M. C.; Farkas, O.; Malick, D. K.; Rabuck, A. D.; Raghavachari, K.; Foresman, J. B.; Ortiz, J. V.; Cui, Q.; Baboul, A. G.; Clifford, S.; Cioslowski, J.; Stefanov, B. B.; Liu, G.; Liashenko, A.; Piskorz, P.; Komaromi, I.; Martin, R. L.; Fox, D. J.; Keith, T.; Al-Laham, M. A.; Peng, C. Y.; Nanayakkara, A.; Challacombe, M.; Gill, P. M. W.; Johnson, B.; Chen, W.; Wong, M. W.; Gonzalez, C.; Pople, J. A. *Gaussian 03*, revision B.04; Gaussian, Inc.: Wallingford, CT, 2004.
- (40) Werner, H.-J.; Knowles, P. J.; Lindh, R.; Manby, F. R.; Schütz, M.; Celani, P.; Korona, T.; Rauhut, G.; Amos, R. D.; Bernhardsson, A.; Berning, A.; Cooper, D. L.; Deegan, M. J. O.; Dobbyn, A. J.; Eckert, F.; Hampel, C.; Hetzer, G.; Lloyd, A. W.; McNicholas, S. J.; Meyer, W.; Mura, M. E.; Nicklass, A.; Palmieri, P.; Pitzer, R.; Schumann, U.; Stoll, H.; Stone, A. J.; Tarroni, R.; Thorsteinsson, T. *MOLPRO, a package of ab initio programs*, Version 2002.
- (41) Cheesman, A. Ph. D. Dissertation, University of Bristol, 2006.
- (42) Kang, J. K.; Musgrave, C. B. *J. Chem. Phys.* **2001**, *115*, 11040.

(43) Gurvich, L. V.; Veyts I. V.; Alcock, C. B. *Thermodynamic Properties of Individual Substances*, 4th ed.; Hemisphere Pub. Co.: New York, 1989.

(44) Frenkel, M.; Marsh, K. N.; Wilhoit, R. C.; Kabo, G. J.; Roganov, G. N. *Thermodynamics of Organic Compounds in the Gas State*; Thermodynamics Research Center: College Station, TX, 1994.

(45) Harris, S. J.; Goodwin, D. G. *J. Phys. Chem.* **1993**, 97, 23.

(46) Skokov, S.; Weiner, B.; Frenklach, M.; Frauenheim, Th.; Sternberg, M. *Phys. Rev. B* **1995**, 52, 5426.

(47) Harvey, J. N. *Phys. Chem. Chem. Phys.* **2007**, 9, 331.

(48) Michl, J. *J. Am. Chem. Soc.* **1996**, 118, 3568, and references cited therein.

JP8034538